CrossMark

ORIGINAL ARTICLE

Electrodeposition of Electroactive Co–B and Co–B–C Alloys for Water Splitting Process in 8 M NaOH Solutions

Dawid Kutyła[1] · Maciej Palarczyk[1] · Karolina Kołczyk[1] · Remigiusz Kowalik[1] ·
Piotr Żabiński[1] ◉

Abstract The aim of this work was to determine parameters of obtaining Co–B and Co–B–C alloys characterized by low overpotential in hydrogen evolution reactions. There were tests performed to examine the influence of borax and arginine concentration changes as well as the value of cathodic current intensity on the composition, morphology, synthesis current efficiency, and effectiveness of hydrogen evolution. Carbon was added to Co–B alloys to improve its properties of water decomposition in 8 M NaOH solution at 90 °C. The results of the experiments confirmed a decrease in overpotential values from 48 mV/dec for Co–8.5B alloy to 33 mV/dec for Co–8.2B–9.6C alloy obtained at the highest concentration (0.1 M) of arginine in the electrolyte. It was observed that alloys of good catalytic properties featured an amorphous structure. The coatings were analyzed with the use of a scanning electron microscope (SEM) and X-ray diffraction (XRD). The content of boron was assessed based on the glow discharge spectroscopy (GDS) method, whereas carbon was analyzed with the method of adsorption spectroscopy of infrared radiation.

Keywords Electrodeposition · Hydrogen evolution · Cobalt alloys · Non-noble metals catalyst · Metal–carbon alloys

✉ Piotr Żabiński
zabinski@agh.edu.pl

[1] Faculty of Non-Ferrous Metals, AGH University of Science and Technology, al. A. Mickiewicza 30, Krakow, Poland

Introduction

Recently, there has been more and more focus on the development and implementation of environmentally friendly technologies. One of the concepts elaborated by Japanese scientists is the application of sustainable energy in the form of methane through electrolytic production of hydrogen [1–3]. It relies on utilization of CO_2 generated by mankind to methane. The source of the hydrogen essential in this reaction will be gaseous H_2 obtained in the process of seawater electrolysis. The electrolysis will be powered by current generated by solar panels. The obtained methane can be easily transported, stored, or converted into other energy carriers. One of the key materials required in this technological process are cathodes for hydrogen production.

One of the currently applied electrode materials in industrial production of hydrogen is metallic nickel and Ni-based alloys [4–6]. It mainly results from their good catalytic properties and relatively low cost in comparison to highly active but expensive platinum metals. Improvement of catalytic efficiency can be done through creation of alloys characterized by the presence of phases of low hydrogen evolution overpotential. One of the possible solutions is the creation of platinum metal alloys with nickel or cobalt—Ni–Pd [7, 8], Co–Pd [9], Co–Rh [10], and Co–Ru [11, 12]—which enables to lower the content of expensive metals in the electrode while maintaining very good properties. Addition of molybdenum or tungsten allows to lower both the value of overpotential and corrosive resistance in comparison to pure Ni or Co [13–17]. Moreover, in many cases, the presence of a magnetic field during synthesis can also decrease the overpotential [18–20]. It was also found that addition of carbon in alloys of cobalt

with molybdenum significantly lowered the energy of electrons bonds Co $2p^{3/2}$ and Mo $3d^{5/2}$.

It means transfer of the charge from carbon to metal in alloy and causes a faster transfer of the charge from metal to the hydrogen atom and thus acceleration of the hydrogen evolution process on such an alloy. This phenomenon also takes place in the case of alloys Ni–Mo–C, Co–W–C, and Ni–Fe–C [21–24]. Combining nickel, molybdenum or cobalt, and non-metals into semiconducting compounds Ni–S [25], Co–Se [26], Mo–Se [26, 27], and Mo–S [28] has been intensely investigated recently. It results from a low price of the metals and their wide accessibility while maintaining catalytic properties close to the platinum group of metals.

The work presents test results concerning electrochemical synthesis of Co–B alloys. They featured good electrocatalytic properties. Moreover, addition of carbon in the form of arginine to the bath allowed to obtain Co–B–C alloys which presented higher electrochemical activity at increased corrosive resistance.

Experimental Part

The base electrolyte was made by dissolving cobalt sulfate ($CoSO_4 \cdot 7H_2O$), ascorbic acid ($C_6H_8O_6$), ammonium chloride (NH_4Cl), sodium lauryl sulfate (SLC), and saccharine in distilled water. In order to obtain Co–B alloys, 0–0.15 M of borax ($Na_2B_4O_7 \cdot 10H_2O$) was added to the base electrolyte. The source of carbon was from 0.001 to 0.1 M of arginine added to the electrolyte during electrodeposition of Co–B–C alloys. Arginine can dissociate in water and create electroactive ions, which can be a precursor for carbon electrodeposition.

The composition of the base electrolyte is found in Table 1.

The electrochemical processes were realized on the potentiostat Bio-Logic SP-200 equipped with EC-LAB software. Electrodeposition was performed in a measuring cell where the anode was a platinum sheet of 6 cm^2 area, and the deposition process was conducted on previously etched copper plates of 2.8 cm^2. The distance between electrodes is approximately 7 cm. Preparation of the working electrode relied on chemical polishing in a mixture of concentrated acids H_3PO4, HNO_3, and CH_3COOH in a volume relation of 1:1:1 at temperature 65 °C for 45 s.

Table 1 Composition of the base electrolyte

Electrolyte component	Concentration [M]
$CoSO_4$	0.2
$C_6H_8O_6$	0.2
NH_4Cl	0.2
SLC	0.0003
Saccharine	0.005

The obtained alloys were analyzed with regard to the content of cobalt, boron, and carbon. The cobalt content was determined with the EDS method while for boron, the glow discharge spectroscopy (GDS) method (Jobin Yvon, 10,000 RF) was applied, whereas the content of carbon was assessed by burning and then analyzing with absorption spectroscopy of infrared radiation.

Morphology of the deposited alloy surface was examined with the scanning microscope Philips XL30. The phase composition of the cathodic deposition was assessed with the use of X-ray diffraction analysis applying filtered X-rays Cu Kα. The size of the cathodic deposit grains was estimated from the half-width of the peak of the intensity of Cobalt-fcc[111] using the Scherrer equation.

Catalytic activity of the obtained alloys was tested during cathodic evolution of hydrogen in 8 M NaOH at temperature of 90 °C. The reference electrode was a calomel electrode, whereas the anode was a platinum sheet of 6 cm^2 area. The process of hydrogen evolution was carried out on a specially designed plastic container. The material of the cell has good resistance against strong alkaline environment. Directional coefficients of the lines obtained in galvanostatic polarization measurements were determined.

Results and Discussion

Obtaining Co–B Alloys

The Co–B alloys were from the base electrolyte to which borax was added (0–0.15 M). Moreover, sodium lauryl sulfate (SLC) and saccharine were added to the electrolyte. For the prepared solutions, the process of electrolysis was conducted for 2 h for three different current densities (250, 500, and 1000 A/m^2).

On the basis of the obtained experimental data, it can be observed that the increase in the current density is accompanied by a decrease in cathodic current efficiency.

This parameter has been calculated base on the Faraday's Law, which can be expressed as

$$\varphi = \frac{\Delta m}{m} \cdot 100\%$$

$$m = (j \cdot t) \Big/ F \left(\frac{2 \cdot m_{Co}}{m_C} + \frac{4 \cdot m_C}{m_C} + \frac{3 \cdot m_B}{m_B} \right)$$

where

φ –	cathodic efficiency [%]
Δm	mass of deposited coating [g]
m	theoretical mass, based on Faraday's law [g]
J	current intensity [A]
t	time of electrodeposition [s]
F	Faraday's constant [C]

m_{Co}, m_C, m_B mass of cobalt, boron, and carbon in coating [g]

$M_{Co}, M_C,$ molar mass of cobalt, boron, and carbon
M_B [g/mol]

Figure 1 shows that the lowest cathodic current efficiency was achieved for current density of 1000 A/m². It was also noticed that the increase of borax concentration in the electrolyte is followed by an increase of cathodic current efficiency up to a borax concentration of 0.1 M, and then for a concentration of 0.15 M, it decreases. The highest cathodic current efficiency of the electrodeposition process amounting at 89.5% was obtained for a current density of 250 A/m² and for the solution of the highest concentration of borax (0.15 M). For higher densities of the current, the highest cathodic current efficiencies within 60–70% were obtained for solutions containing respectively 0.075 and 0.1 M of borax.

On the basis of the data shown in Fig. 2, it can be noticed that the maximal content of boron that can be achieved in the alloy amounts at about 10% (at.) at a boron salt concentration of 0.075 M for a current density of 500 A/m². The lowest content of boron in the alloy was obtained for a current density of 250 A/m², and the highest for 500 A/m². Moreover, the increase of cathodic current efficiency is connected with an increase of boron content in the alloy, within individual measurement series.

Structure of Co–B Alloys

For all the obtained alloys, the diffraction X-ray analysis was conducted applying filtered X-ray radiation Cu Kα. The figures present diffractograms of cathodic deposits of Co–B alloys deposited from solutions of borax concentrations from 0
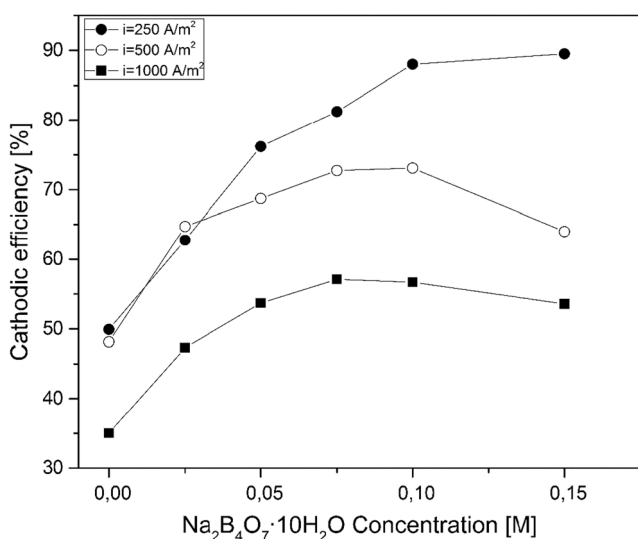

Fig. 1 Dependence of cathodic current efficiency during deposition of the Co–B alloys from electrolyte solutions containing different concentrations of borax (0–0.15 M). Duration of the electrolysis, 2 h
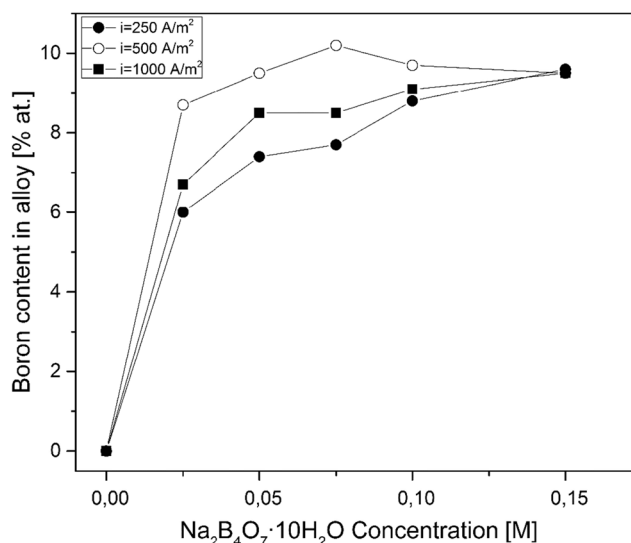

Fig. 2 Dependence of boron content on the coating during deposition of Co–B alloy from electrolytes containing different concentrations of borax (0–0.15 M). Duration of the electrolysis, 2 h

to 0.15 M for three different cathodic current densities (250, 500, and 1000 A/m²).

Grain sizes for individual samples were estimated from diffractograms of cathodic deposits of Co–B alloys through an analysis of the peak half-width of Miller indicators [111] for a regular face-centered cubic structure. For alloys of amorphous structure, the crystalline size was assessed from the half-width of the blurred peak present on the diffractograms.

Figure 3 shows the diffractograms obtained with varied concentrations of borax in the electrolyte. The sizes of obtained crystallites are changing from 8.7 to 2.1 nm. Deposits of Co–B alloys obtained from electrolytes containing 0–0.05 M of borax featured a nanocrystalline regular face-centered cubic structure of lattice plane indicators [111]–[220]. On each diffractogram, there is a peak visible at $2\theta = 44.5°$ and a peak at $2\theta = 76.18°$ which is connected with the regular face-centered cubic structure of the obtained alloys. An increase of borax content in the electrolyte is accompanied by occurrence of peaks at about $2\theta = 44.5$ and $2\theta = 47.14$ indicating that we have a mixture of fcc and hcp structures of cobalt, and a peak at 41.82 indicating a formation of a CoB[111] phase. For samples obtained in the electrodeposition process while applying cathodic current density of 250 A/m² (Fig. 3a), the increase of borax content caused a gradual decrease in the crystal size to 2.1 nm for the content of 0.15 g/l and creation of an amorphous structure on the basis of a hexagonal structure. For diffractograms of cathodic deposits of Co–B alloys deposited at a current density of 500 A/m² (Fig. 3b), a regular face-centered cubic structure with a concentration of 0–0.05 M borax is visible. Further increase of borax salt concentration (0.05–0.1 M) in the electrolyte resulted in a decrease in the size of deposit crystallites from 4.6 to 2.9 nm. There was
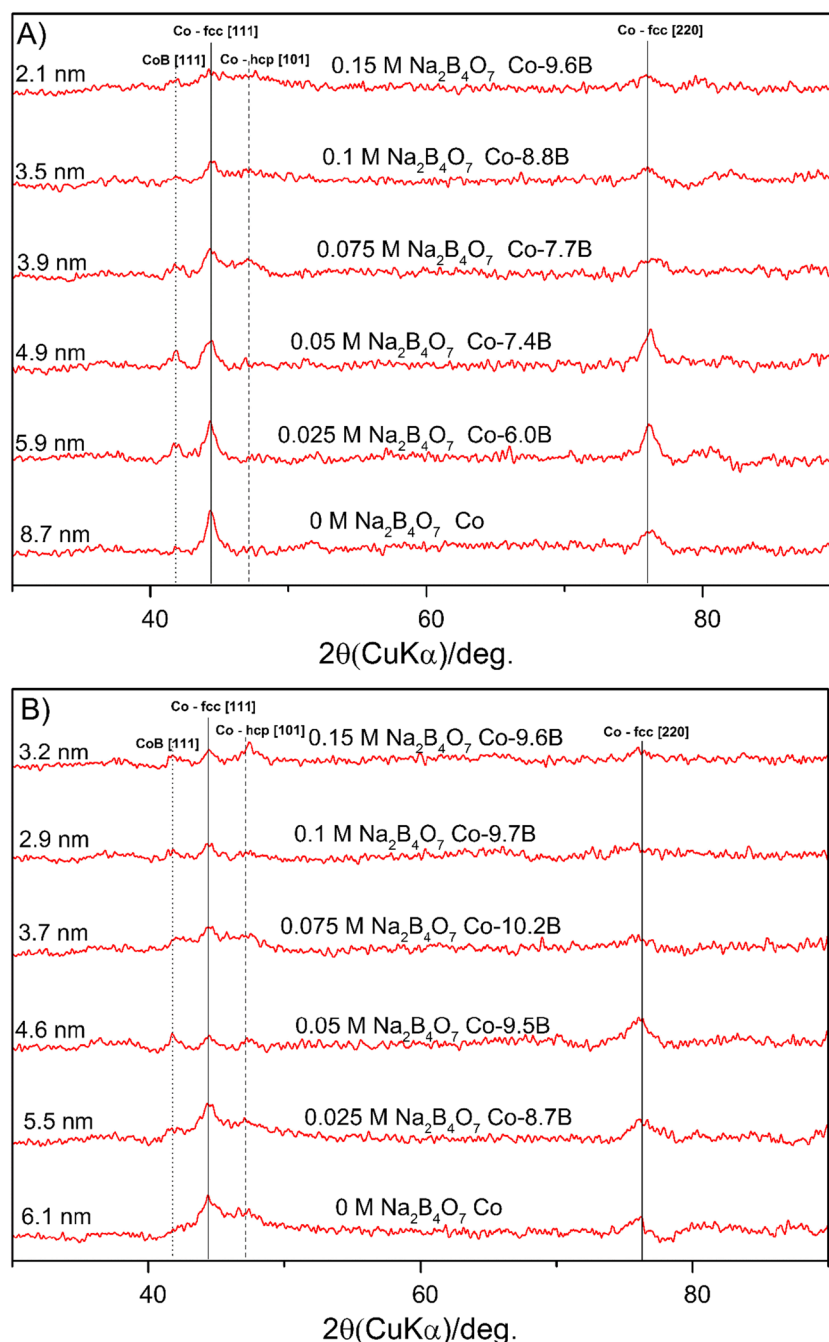
Fig. 3 Diffraction analysis of Co–B alloys obtained from solutions of different borax concentrations in the electrolyte for current densities: **a** 250 A/m^2, **b** 500A/m^2, **c** 1000 A/m^2

observed a change in the face-centered cubic structure into a hexagonal one, which creates a mixture with the CoB[111] phase.

For samples obtained in the electrodeposition process for a current density of 1000 A/m^2 (Fig. 3c), occurrence of peaks originating from the fcc structure was noticed. Also, a transition from a hexagonal structure into an amorphous one was observed. The crystal size for deposited pure cobalt was decreased from 6.4 to 2.3 nm. Addition of borax to the electrolyte caused an increase in their size to 4.9 nm for the Co–8.5B

alloy, and then the size fell to 2.3 nm which is connected with a change of the structure from hexagonal to amorphous.

The surface morphology of the deposited alloys was also examined with the use of a scanning microscope. Table 2 presents microstructures of cathodic deposits of the Co–B alloys obtained from electrolytes of different borax content. The alloys were deposited at three different current densities—250, 500, and 1000 A/m^2.

The analysis of the SEM images indicates a high correlation of the alloy grain shape and the applied current density in
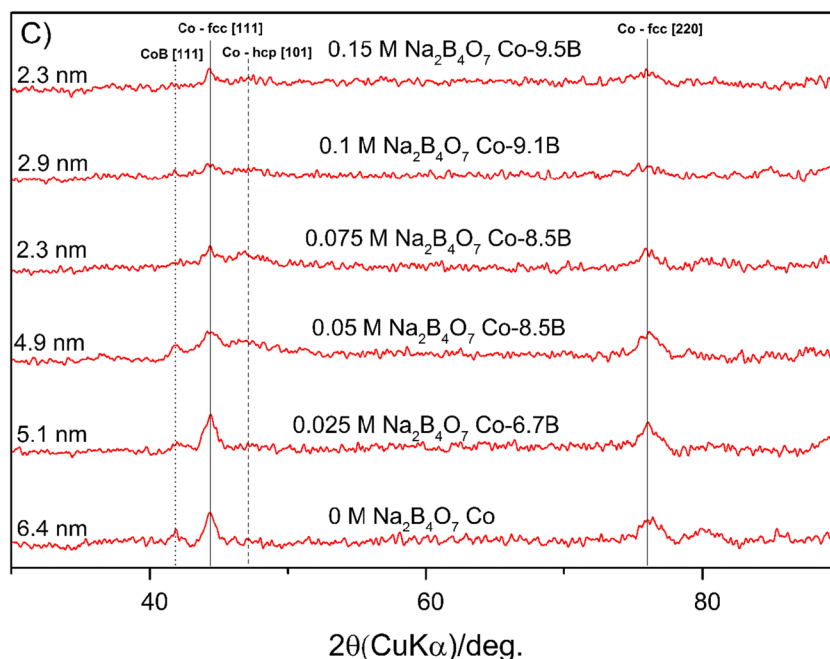
Fig. 3 (continued)

the electrodeposition process, whereas the grain size is determined by concentration of borax in the electrolyte used in the deposition process. The presented images were taken at ×500 magnification. The cathodic deposit is compact and homogeneous; there are no cracks on it. For current density of 250 A/m^2, the grain size is growing with the increase of borax concentration in the electrolyte used to obtain the Co–B alloy until reaching a size of 20 μm for a solution of the highest concentration of borax (0.15 M).

For coatings obtained at a current density of 500 A/m^2, the grains are very small for 0.05 M of borax in the electrolyte. For 0.1 M of borax, creation of bigger clusters of deposited alloy is observed. An increase in borax content makes the structure more irregular with a grain size around 30–40 μm which is visible for a concentration of 0.15 M.

For the highest applied current density of 1000 A/m^2, the grain shape is irregular. An increase of borax concentration in the electrolyte is accompanied by a more and more expanded structure, and grain borders are clearly visible. The grain size changes sharply with an increase of borax concentration in the electrolyte which results from a change of the structure and the intensity of hydrogen evolution, which have a strong impact for surface development.
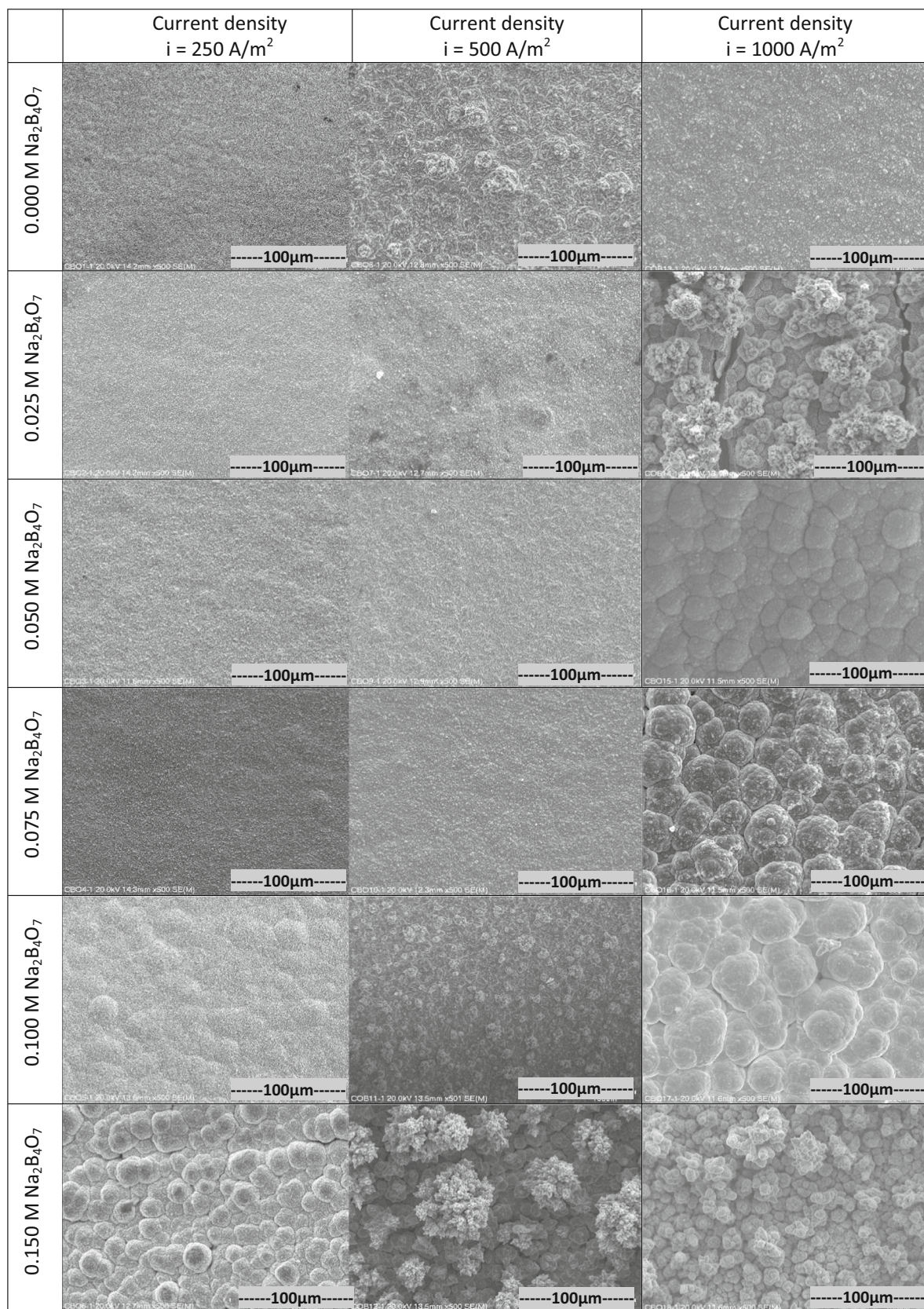
Hydrogen Evolution of Co–B Alloys

The change in boron content in the Co–B alloy as well as the structure change of the obtained alloy probably significantly influence the alloy's electrocatalytic properties. In order to follow the changes, tests were made conducted on hydrogen evolution on Co–B alloys at 90 °C in 8 M NaOH.

Figure 4 shows test results of Co–B alloy activity in the process of hydrogen evolution at 90 °C with 8 M NaOH. The curves were obtained in galvanostatic measurements of Co–B alloys deposited from electrolytes of different borax concentrations (Na$_2$B$_4$O$_7$·10H$_2$O) for three different cathodic current densities (250, 500, and 1000 A/m^2).

Polarization curves comprise two sections of different directional coefficients of the Tafel equation. The first area of the polarization curve is the area of the examined inclination of the Tafel slope in the process of hydrogen evolution at low current densities. The second area of the polarization curve is the area in which the basic conditions of the Tafel slope occurrence are not met. Hydrogen evolution on this area takes place violently.

An analysis of curves for Co–B alloys deposited on galvanostatic mode from solutions of different borax concentrations at a density 250 A/m^2 (Fig. 4a) suggests that an increase in boron content in the alloy changes the inclination of the Tafel slope from 123 mV/dec for Co–7.4B alloy to 69 mV/dec for the alloy of the highest borax concentration in the electrolyte. It indicates differences in alloy activity for different borax contents. An increase in boron content positively influenced catalytic properties. The mechanism of hydrogen evolution process is not defined and depends on the surface morphology and occurrence of domains of nanocrystalline and amorphous structures. For alloys obtained at a current density of 500 A/m^2 (Fig. 4b), it is visible that an increase in borax content in the electrolyte used for obtaining Co–B alloys does not influence the alloy catalytic activity. Inclination of the Tafel slope is constant and amounts at 160 mV/dec. For the highest current density of 1000A/m^2 (Fig. 4c), the galvanostatic curves

Table 2   SEM micrographs of Co–B alloys electrodeposited for 2 h in base electrolyte (0.2 M CoSO$_4$·7H$_2$O) with different concentrations of Na$_2$B$_4$O$_7$

	Current density i = 250 A/m^2	Current density i = 500 A/m^2	Current density i = 1000 A/m^2
0.000 M Na$_2$B$_4$O$_7$			
0.025 M Na$_2$B$_4$O$_7$			
0.050 M Na$_2$B$_4$O$_7$			
0.075 M Na$_2$B$_4$O$_7$			
0.100 M Na$_2$B$_4$O$_7$			
0.150 M Na$_2$B$_4$O$_7$			

Used magnification: ×500
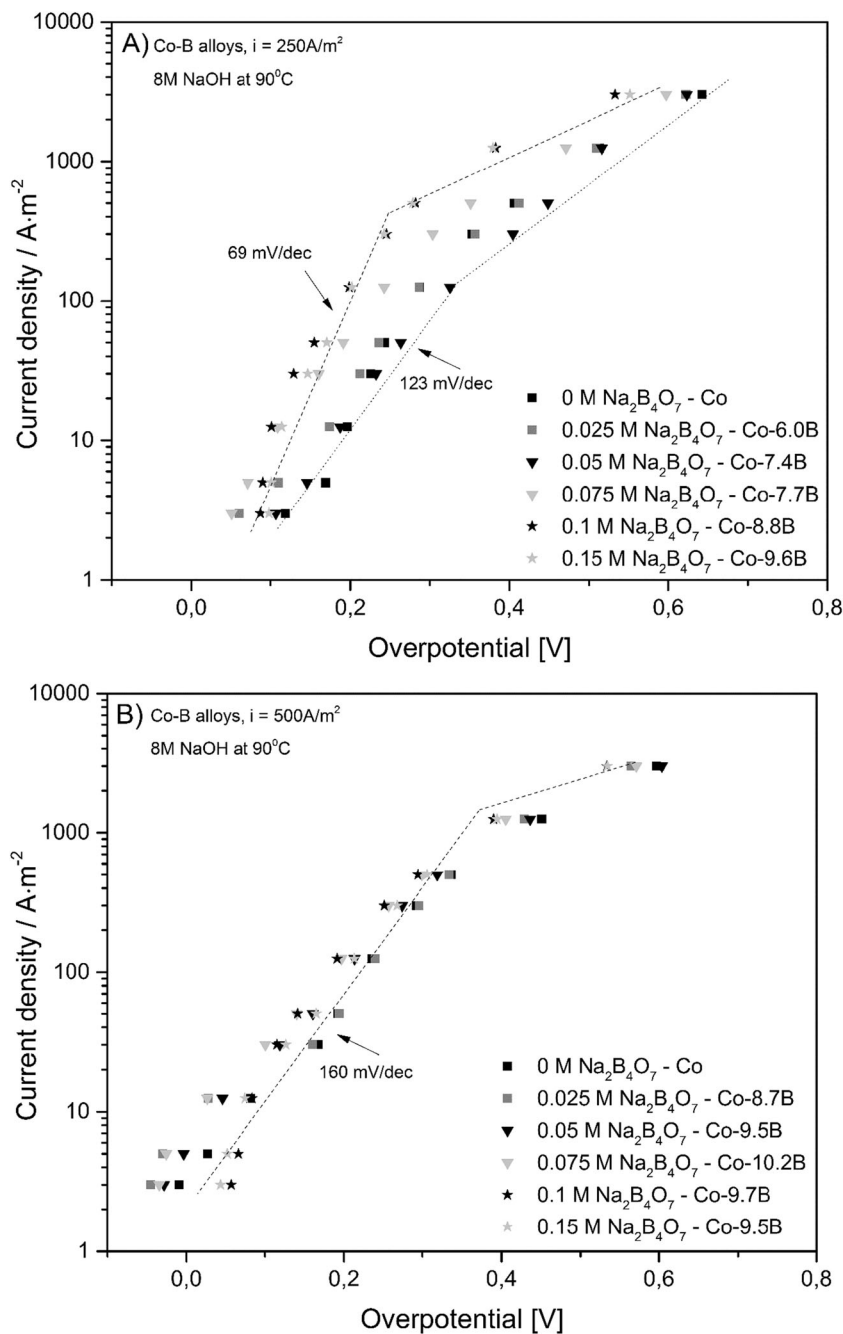
Fig. 4 Galvanostatic curves of Co–B alloys obtained from solutions of different borax concentrations in the electrolyte for current densities: **a** 250 A/m², **b** 500A/m², **c** 1000 A/m²

show that the best catalytic properties are found in the Co–8.5B alloy as the Tafel slope inclination is the lowest and amounts at 48 mV/dec. It was obtained from a solution of 0.075 M borax concentration in the electrolyte. Further increase in borax concentration in the electrolyte caused an increase of the Tafel slope inclination and subsequent worsening of catalytic properties. In the discussed case, the Tafel slope inclination is close to the value of 35 mV/dec; therefore, it can be claimed that the slowest phase is the recombination of two

adsorbed hydrogen atoms with creation of hydrogen molecules. The increase of the catalytic properties is due the mixture of amorphous Co and CoB phases with lover overpotential of hydrogen evolution present. We have to take into consideration that the irregular agglomerates shown on SEM images for 0.15 M of borax in electrolyte obtained in the highest current density can be connected with improvement of the catalytic properties. Their shape is very well-developed, and it is increasing the active center on the surface of the
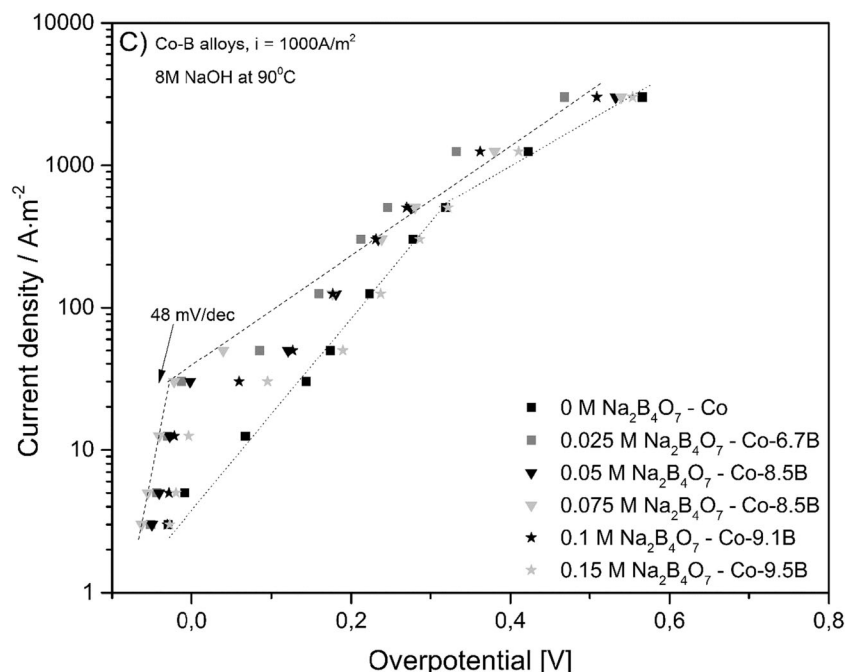
Fig. 4 (continued)

electrode. Moreover, the hydrogen evolution reaction takes place during the synthesis which can affect the surface evolution process.

Obtaining of Co–B–C Alloys

The Co–B–C alloys were obtained in the process of electrodeposition from the electrolyte containing aqueous solutions of cobalt sulfate ($CoSO_4 \cdot 7H_2O$, 0.2 M), ascorbic acid ($C_6H_8O_6$, 0.2 M), ammonium chloride (NH_4Cl, 0.2 M), borax ($Na_2B_4O_7 \cdot 10H_2O$, 0.1 M), and arginine concentrated from 0 to 0.1 M. Moreover, sodium lauryl sulfate (SLC) and saccharine were added to the electrolyte. For the prepared solutions, the process of electrolysis was conducted for 2 h for three applied current densities (250, 500, and 1000 A/m²).

On the basis of the obtained experimental data (Fig. 5), it can be observed that an increase in current density causes a decrease in cathodic current efficiency. The highest cathodic current efficiency of the electrodeposition process amounting at 86.68% was achieved for a current density of 250 A/m² and for the solution without arginine. A slight addition of arginine (0.001 M) to the electrolyte caused a sharp fall of cathodic current efficiency from 86.68 to 73% in the process of electrodeposition, whereas next additions caused a gradual increase in cathodic current efficiency from 73% until reaching the value of about 80% for three solutions of the highest arginine content. For current density at 500 A/m², cathodic efficiency stayed at 60% regardless of arginine concentrations in the electrolyte. The lowest cathodic current efficiency was

achieved in the electrolyte while applying a current density of 1000 A/m².

The obtained alloys were analyzed with regard to the percentage content of carbon by burning and then analyzing with the method of adsorption spectroscopy of infrared radiation. A correlation of carbon content in the alloy and arginine concentration in the electrolyte was indicated (Fig. 6). The highest content of carbon in the alloy was achieved by electrodeposition from the electrolyte of arginine concentration at 0.1 M and the highest current density, and it was 11.41% (at.). An
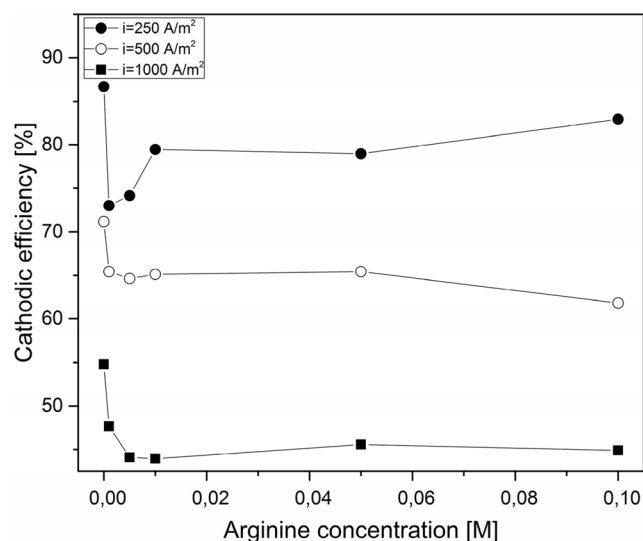

Fig. 5 Dependence of cathodic current efficiency for Co–B–C alloys obtained from electrolyte containing different concentrations of arginine (0–0.1 M). Time of the electrolysis, 2 h
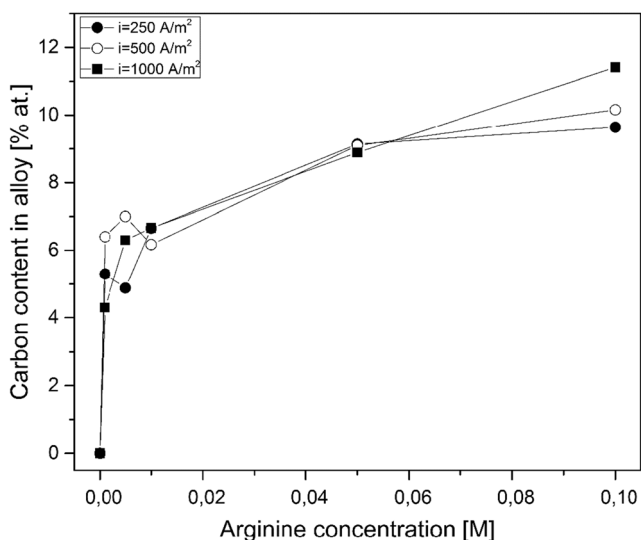
Fig. 6 Dependence of carbon content on Co–B–C alloys obtained from electrolyte containing different concentrations of arginine (0–0.1 M). Time of the electrolysis, 2 h

increase in arginine concentration in the electrolyte caused an increase of carbon for all applied current densities. Their values were similar for each concentration of the solution regardless of the applied current density.

Moreover, correlation of boron content and arginine concentration in the electrolyte was analyzed (Fig. 7). A slight amount of arginine (0.001–0.002 M) caused a significant decrease in boron content in the deposit. A gradual increase of boron was observed depending on the arginine content, but it was strongly correlated with the applied current density.
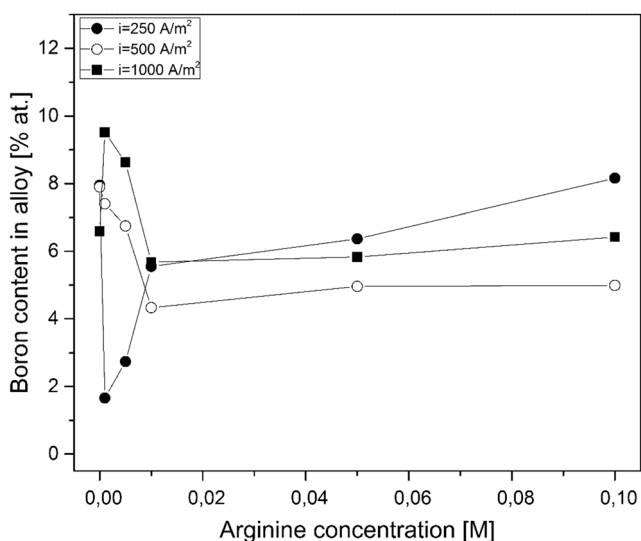

Fig. 7 Dependence of boron content on the coating for Co–B–C alloys obtained from electrolyte containing different arginine concentrations (0–0.1 M). Time of the electrolysis, 2 h

Structure of Co–B–C Alloys

Figure 8 shows diffractograms of cathodic deposits of Co–B–C alloys deposited from solutions containing an arginine of concentration of 0–0.1 M. The crystal size for individual samples was defined from diffractograms of cathodic deposits of Co–B–C alloys by an analysis of the half-width of peaks of Miller indicators [111] for an fcc structure.

In Fig. 8a, the increase in arginine concentration in the electrolyte for alloys deposited at a current density of 250 A/m^2 caused an increase in crystalline size from 4.5 to 5.6 nm for a concentration of 0.005 M. Then, a sharp fall of the crystal size to 2.8 nm for the Co–5.6B–6.6C alloy was observed. It is connected with the increase in boron content in the alloy. Next, a gradual increase in Co crystal size is observed at 4.9 nm for an alloy deposited from the electrolyte of the highest concentration of arginine 0.1 M. For the Co–1.7B–5.3C alloy, an amorphous structure was observed. An increase of carbon in the alloy makes the structure to become a mixture of amorphous and hexagonal structures. Further increase in carbon content in the alloy causes a transition of amorphous structure into a hexagonal one for an alloy deposited from the solution of the highest arginine concentration.

In the case of current density of 500 A/m^2 (Fig. 8b), the increase of arginine in the electrolyte causes an increase in crystal size from 2.0 nm for the Co–9.7B alloy to 3.5 nm for the Co–5.0B–10.2C alloy. It results from the creation of an amorphous structure for the Co–6.8B–7.0C alloy. Further increase of arginine concentration in the electrolyte for obtaining Co–B–C alloys caused a gradual increase of the grain size. It is connected with occurrence of a hexagonal structure on the basis of the amorphous one. An increase in carbon content in the alloy is accompanied by an increase of the hexagonal structure participation in the alloy structure to finally transit into it completely for Co–5.0B–10.2C.

Co–B–C alloys deposited from solutions of arginine concentration from 0 to 0.1 M for current density 1000A/m^2 are characterized by an amorphous structure which is clearly seen for Co–9.5B–4.3C and Co–8.6B–6.3C alloys deposited from solutions of arginine concentration from 0.001 to 0.005 M. Further increase of arginine concentration in the electrolyte causes an increase of crystalline size up to 4.6 nm for the alloy of the highest content of carbon. It is caused by occurrence of a hexagonal structure on the basis of the amorphous one for the Co–5.7B–6.7C alloy. Significant changes occurring in the estimated cobalt crystal size for a current density of 500 and 1000 A/m^2 are likely to result from application of high current density and differentiation of composition of the obtained cathodic deposits. Changes in the crystalline size of alloys obtained during electrodeposition in three applied current densities are visible in SEM photographs obtained with the use of a scanning microscope. But they are creating agglomerates of crystals, and the size of particles is much bigger.
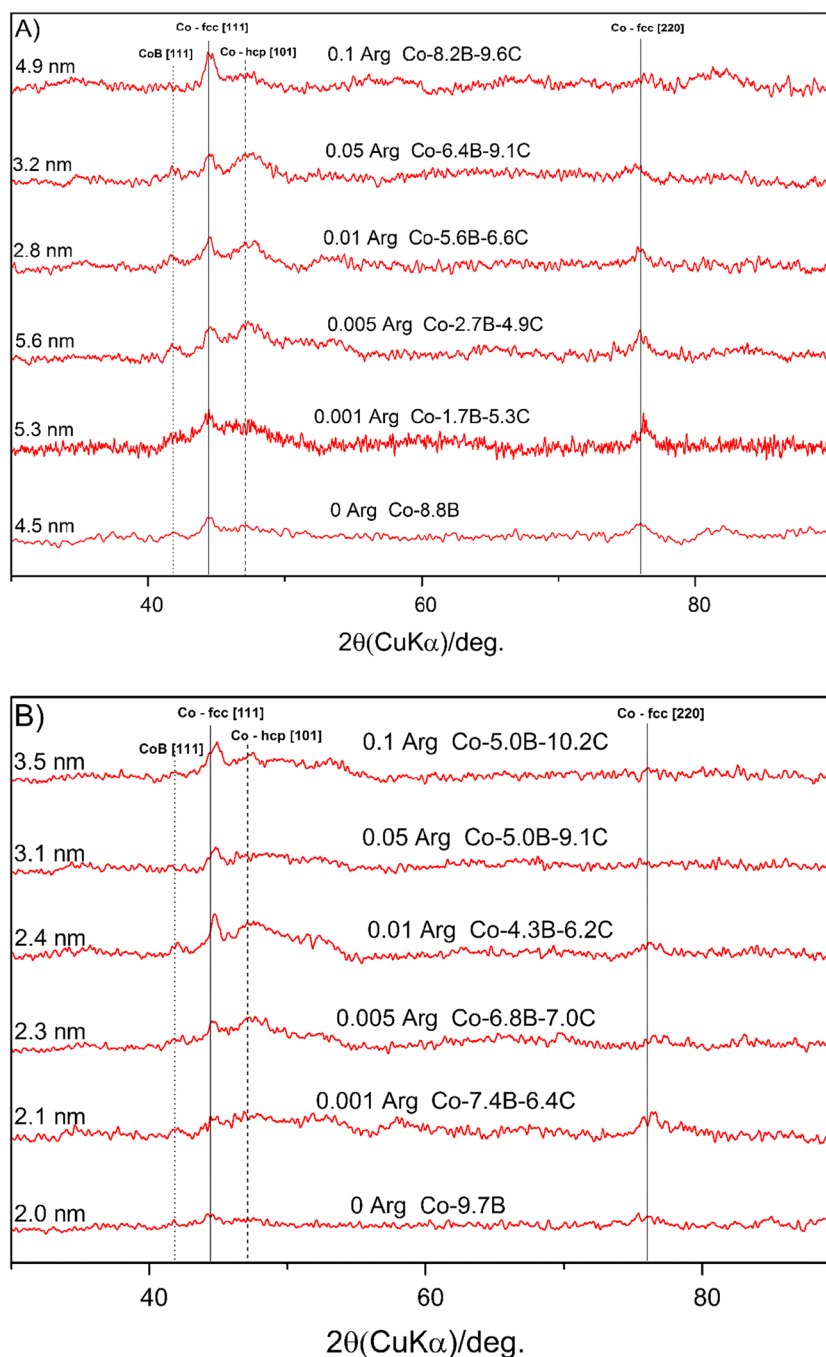
Fig. 8 Diffraction analysis of Co–B–C alloys obtained from solutions of different concentrations of arginine in the electrolyte for current densities: **a** 250 A/m^2, **b** 500A/m^2, **c** 1000 A/m^2

Table 3 presents microstructures of cathodic deposits obtained from electrolytes containing 0.1 M Na$_2$B$_4$O$_7$·10H$_2$O and different concentrations of arginine deposited at a current density of 250, 500, and 1000 A/m^2. For a current density of 250 A/m^2, the increase in arginine content in the electrolyte is accompanied by an increased number of microcracks. It is probably caused by separation of hydrogen blisters created on the cathodic deposit surface. From the arginine concentration of 0.05 M, grain borders are clearly visible, and for the highest concentration (0.1 M), individual spherical grains are seen. The grain size ranges from 10 to 25 μm. Microstructures obtained from alloys deposited at a current density of 500 A/m^2 feature more microcracks, and from the arginine concentration of 0.01 M in the solution, the grain shape and size are visible. For the highest current density of 1000A/m^2, the grains are of irregular shape. Grain borders are
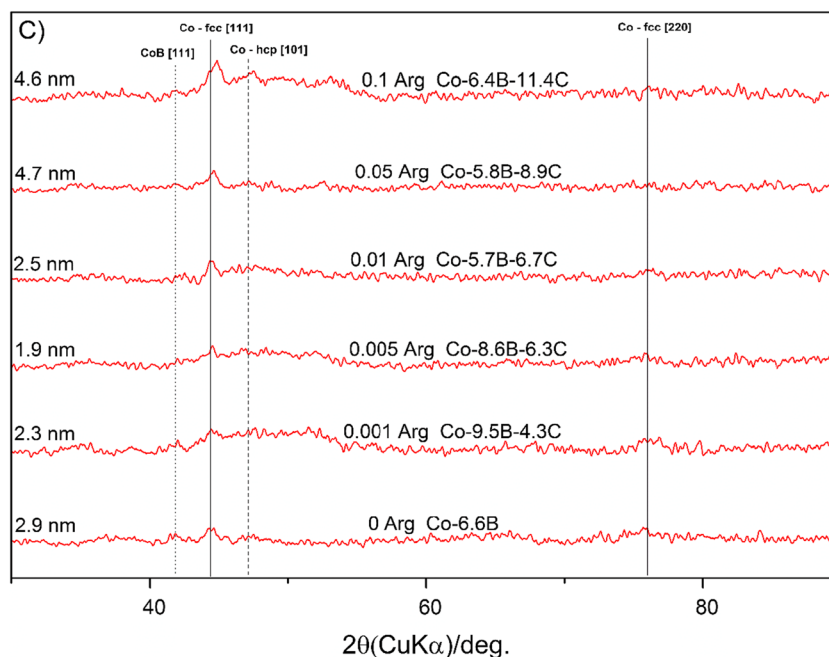
Fig. 8 (continued)

clearly seen, and very tiny grains accumulating into groups can also be seen. For the largest carbon content in the alloy, highly irregular individual grains can be seen.

Hydrogen Evolution on Co–B–C Alloys

Figure 9 presents galvanostatic curves of Co–B–C alloys. In the case of deposition at a current density of 250 A/m^2, an increase of carbon in the alloy caused a difference in alloy activity. The best catalytic properties were found in the Co–8.2B–9.6C alloy of the lowest carbon content. It features the lowest value of the Tafel slope inclination amounting at 33 mV/dec, whereas the highest value of the Tafel slope inclination was observed in the alloy of the lowest carbon content (Co–7.9B–2.4C). It can be deduced that an increase in carbon content in an alloy improves catalytic properties of the alloy. An increase in current density at deposition of Co–B–C alloys affects catalytic properties of the alloys.

The increase in carbon content in the alloy made the points on the galvanostatic curve in the process of hydrogen evolution to move away. It means differences in activities of alloys obtained from electrolytes of different arginine contents. Mechanisms of hydrogen evolution on Co–B–C alloys are the same as on Co–B alloys. For the Co–8.2B–9.6C alloy deposited at a current density of 250 A/m^2, the Tafel slope inclination amounts at 33 mV/dec which means that the slowest phase is the reaction of recombination of two adsorbed adjacent atoms with creation of a hydrogen molecule. For Co–B–C alloys deposited at a current density of 500 A/m^2, the Tafel slope inclination is about 66 mV/dec for

all alloys with arginine. The mechanism of the hydrogen evolution process is not defined, and it depends on morphology and occurrence of domains of amorphous and hexagonal structure in the structure. For alloys deposited at a density of 1000 A/m^2, the Tafel slope inclination varies between 42 and 46 mV/dec for all Co–B–C alloys. It suggests that the slowest phase is the recombination of two adsorbed atoms with creation of a hydrogen molecule. Although Co–B–C alloys were usually of hexagonal structure, addition of carbon to Co–B alloy caused that catalytic properties of the alloys were better than catalytic properties of Co–B amorphous alloys.

The data presented in Table 4 shows the electrochemical activity of some cobalt-based alloys obtained in electrochemical synthesis. Among them, the highest slope of Tafel's line in the activation range was observed for Co–Pd, and it was 25 mV/dec. Very high activity is typical for the noble metals and their alloys with Co and Ni. The slowest step of the hydrogen evolution process is the reaction between two adsorbed protons on the electrode surface. For pure cobalt, the hydrogen evolution mechanism is limited by a simple charge transfer-controlled reaction. A Tafel slope of 145 mV per decade may arise from various reaction pathways depending on the surface coverage of adsorbed hydrogen. Addition of molybdenum, tungsten, and boron can significantly change the mechanism of hydrogen evolution and the recombination of adsorbed hydrogen atoms as the rate-determining step. It is clearly shown for Co–Mo, Co–B, and Co–B alloys, where the Tafel slope is close to 35 mV/dec. Figure 10 shows the

Table 3   SEM micrographs of Co–B–C alloys electrodeposited for 2 h in the electrolyte (0.2 M CoSO$_4$·7H$_2$O, 0.1 M Na$_2$B$_4$O$_7$) with different concentrations of arginine
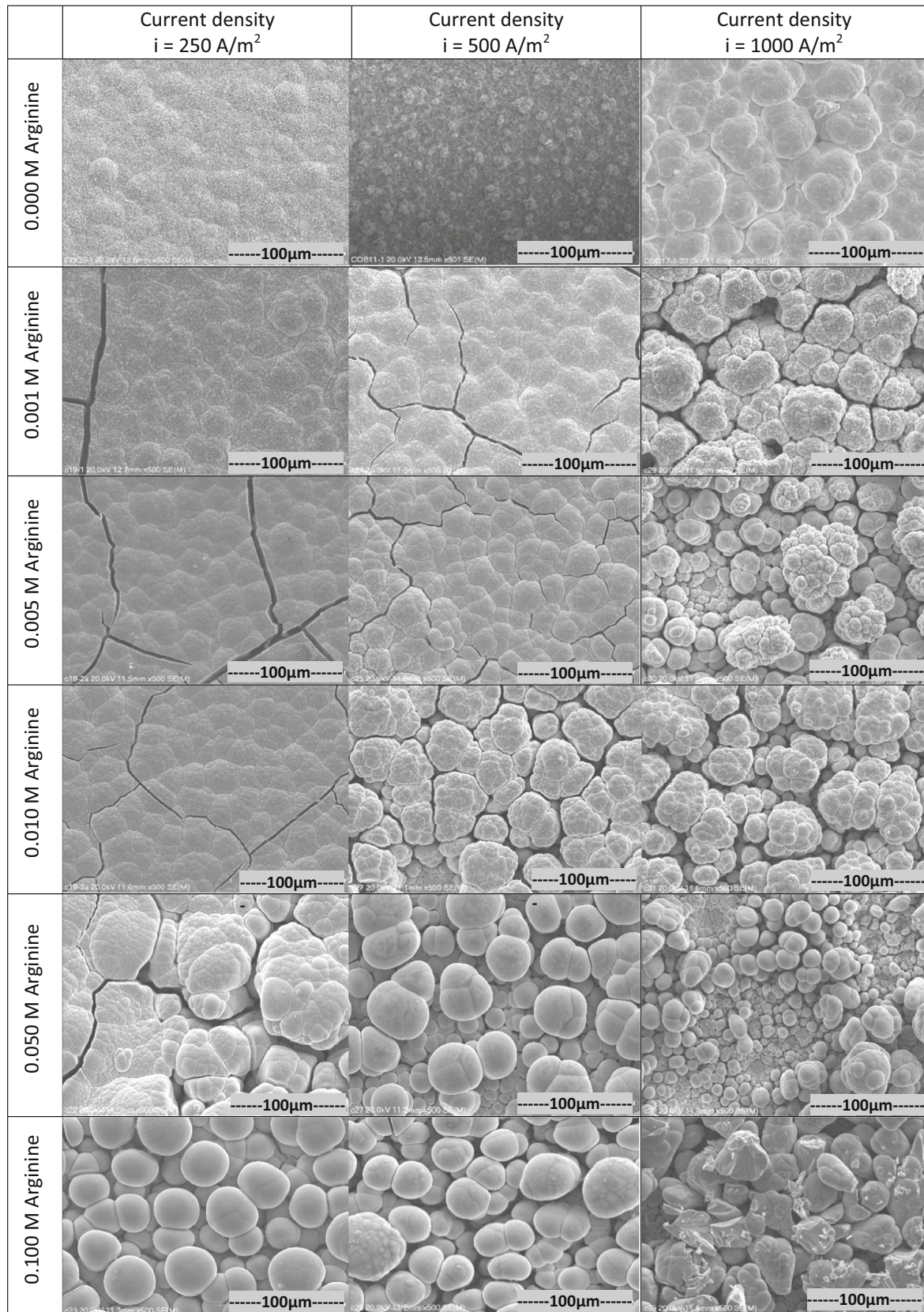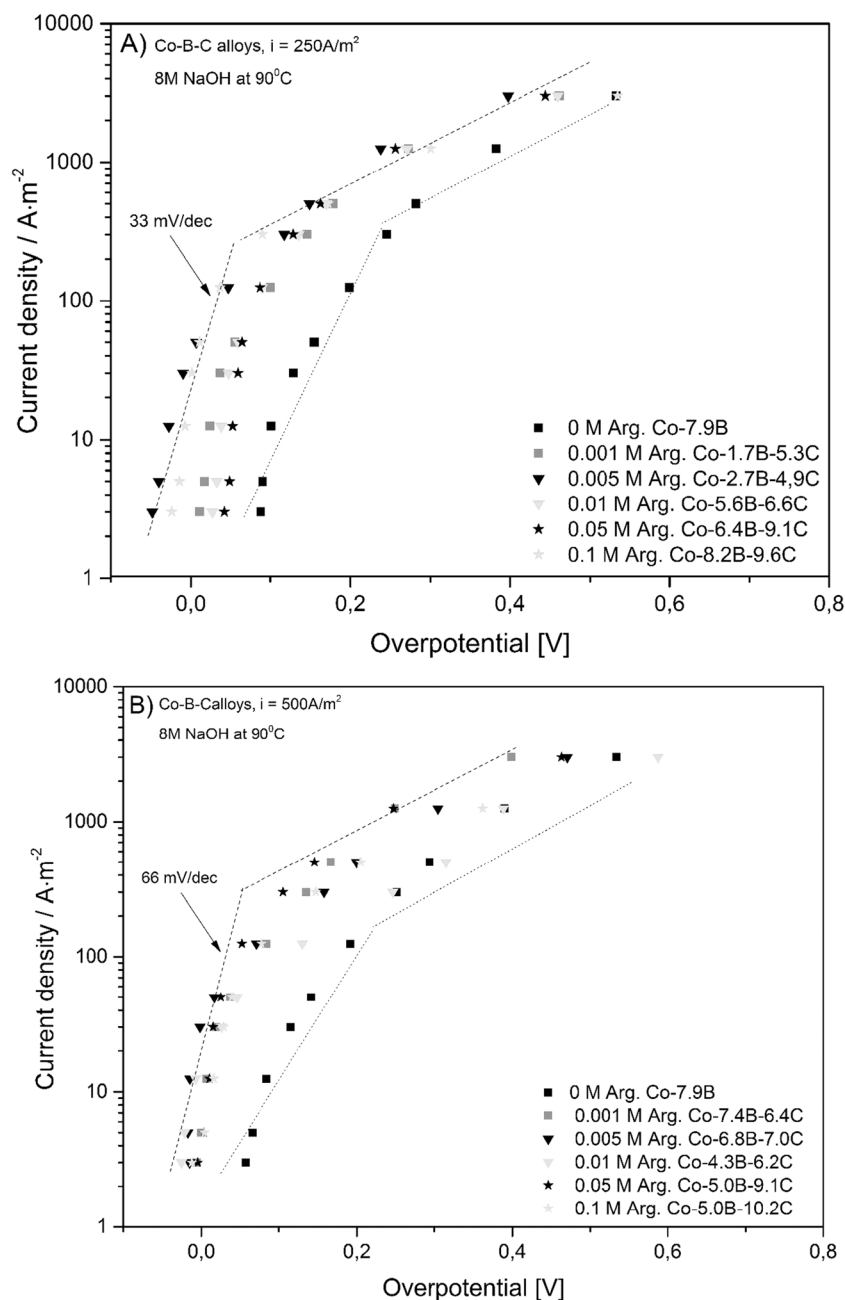

Used magnification: ×500

Fig. 9 Galvanostatic curves of Co–B–C alloys obtained from solutions of different arginine concentrations in the electrolyte for current densities: **a** 250 A/m², **b** 500A/m², **c** 1000 A/m²

comparison between catalytic activity of pure cobalt metal foil, Co–B, and Co–B–C alloys electrodeposited in this study with catalytic activity for HER on platinum foil. Obtained results for the most active ternary cobalt alloy are very close to hydrogen evolution activity on platinum foil. In general, the arginine addition positively influenced the catalytic activity of the obtained alloys in all the cases. The addition of carbon into these binary alloys also significantly decreases the binding energy of 4f7/2 from 32.3 eV for Co–W alloys to 31.0 eV for Co–W–C alloys [20]. This fact suggests that carbon addition can influence the charge

transfer from metal to proton and positively affect electrocatalytic activity.

Conclusions

The conducted experiments allowed to state the following conclusions:

- The best conditions for electrodeposition of Co–B–C alloys were obtained in the electrolyte of 0.1 M borax
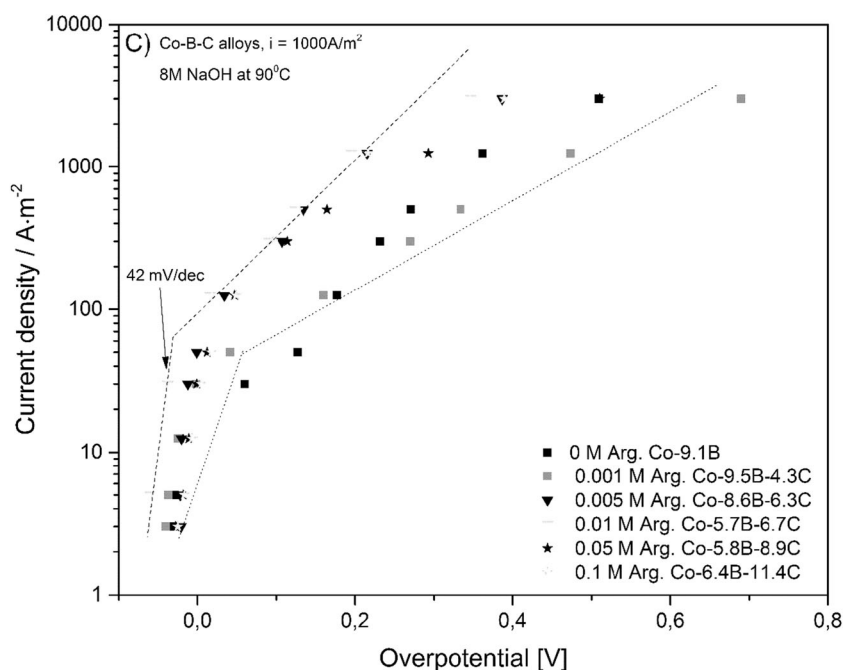
Fig. 9 (continued)

concentration and 0.005–0.05 M of arginine; the obtained alloys were characterized by a mixture of structures: nano-crystalline and amorphous.

· The highest cathodic current efficiencies in the process of Co–B and Co–B–C alloy deposition were observed for current density of 250 A/m^2, at high borax concentrations in the electrolyte.

· Creation of the amorphous structure was observed only for high content of boron in Co–B alloy.

The process of hydrogen evolution on Co–B–C alloys significantly relies on the current density applied to obtain the alloy; the most favorable was applying alloys obtained during deposition at the highest current density; alloys obtained this way featured effective hydrogen evolution, and the phase determining the reaction velocity

was recombination of two adsorbed atoms with creation of a hydrogen molecule.

· Addition of carbon and creation of a three-component alloy Co–B–C improved the alloy activity in the process of hydrogen evolution.

· Addition of carbon decreased the Tafel slope inclination to the value of 33 mV/dec for the Co–8.2B–9.6C alloy and improved efficiency of hydrogen evolution.

Table 4 The hydrogen evolution electroactivity of electrodeposited Co and Co-based alloys in alkaline solutions

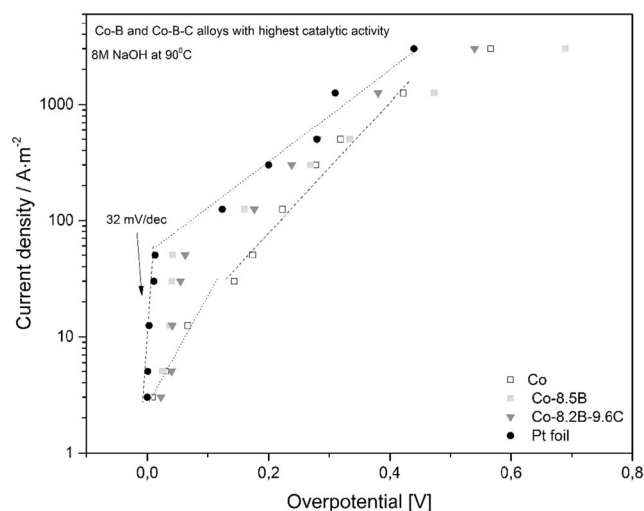| Material	Overpotential [mV/dec]	Solution	Temperature [^{0}C]	Reference
Co-31Pd	25	1M NaOH	25	[9]
Co-Mo29	36	8M NaOH	90	[19]
Co-9W	110	8M NaOH	90	[20]
Co-8.2W-12.5C	35	8M NaOH	90	[20]
Co	145	8M NaOH	90	This work
Co-8.5B	48	8M NaOH	90	This work
Co-8.2B-9.6C	33	8M NaOH	90	This work

Fig. 10 Galvanostatic curves of Co–B and Co–B–C alloys with the highest catalytic activity, electrodeposited Co and Pt foil

References

1. K. Hashimoto et al., The use of renewable energy in the form of methane via electrolytic hydrogen generation. Arch. Metall. Mater. **58**(1), 231–239 (2013)

2. Hashimoto, K., et al., *The production of renewable energy in the form of methane using electrolytic hydrogen generation.* Energy, Sustain. Soc. **4**(1) (2014)

3. K. Hashimoto et al., The use of renewable energy in the form of methane via electrolytic hydrogen generation using carbon dioxide as the feedstock. Appl. Surf. Sci. **388**, 608–615 (2016)

4. K. Lohrberg, P. Kohl, Preparation and use of Raney-Ni activated cathodes for large scale hydrogen production. Electrochim. Acta **29**(11), 1557–1561 (1984)

5. M.P. Marceta Kaninski et al., Energy consumption and stability of the Ni-Mo electrodes for the alkaline hydrogen production at industrial conditions. Int. J. Hydrog. Energy **36**(15), 8864–8868 (2011)

6. M.P. Marceta Kaninski et al., A study on the Co-W activated Ni electrodes for the hydrogen production from alkaline water electrolysis—energy saving. Int. J. Hydrog. Energy **36**(9), 5227–5235 (2011)

7. K. Mech et al., Electrodeposition of NiPd alloy from aqueous chloride electrolytes. Appl. Surf. Sci. **388**, 809–816 (2016)

8. I.Z. Ismagilov et al., Hydrogen production by autothermal reforming of methane over NiPd catalysts: effect of support composition and preparation mode. Int. J. Hydrog. Energy **39**(36), 20992–21006 (2014)

9. K. Mech et al., Electrodeposition of Co-Pd alloys from ammonia solutions and their catalytic activity for hydrogen evolution reaction. J. Appl. Electrochem. **44**(1), 97–103 (2014)

10. K. Mech et al., Electrodeposition of Co-Rh alloys from aqueous acidic chloride electrolytes. Surf. Coat. Technol. **258**, 72–77 (2014)

11. D. Kutya et al., Electrochemical deposition of ruthenium and cobalt-ruthenium alloys from acidic chloride ions containing baths. Arch. Metall. Mater. **61**(3), 1221–1228 (2016)

12. K. Mech et al., Electrochemical deposition of alloys in Ru3+-Co2+-Cl–H2O system. J. Electroanal. Chem. **748**, 76–81 (2015)

13. N.V. Krstajić et al., Electrodeposition of Ni-Mo alloy coatings and their characterization as cathodes for hydrogen evolution in sodium hydroxide solution. Int. J. Hydrog. Energy **33**(14), 3676–3687 (2008)

14. Q. Han et al., A study on pulse plating amorphous Ni-Mo alloy coating used as HER cathode in alkaline medium. Int. J. Hydrog. Energy **35**(11), 5194–5201 (2010)

15. K. Mech et al., Electrodeposition of catalytically active Ni-Mo alloys. Arch. Metall. Mater. **58**(1), 227–229 (2013)

16. A. Kawashima et al., Characterization of sputter-deposited Ni-Mo and Ni-W alloy electrocatalysts for hydrogen evolution in alkaline solution. Mater. Sci. Eng. A **226-228**, 905–909 (1997)

17. P.R. Zabiński, R. Kowalik, M. Piwowarczyk, Cobalt-tungsten alloys for hydrogen evolution in hot 8 M NaOH. Arch. Metall. Mater. **52**(4), 627–634 (2007)

18. Zabinski, P.R., A. Jarek, and R. Kowalik, *Effect of applied external magnetic field on electrodeposition of cobalt alloys for hydrogen evolution in 8M NaOH.* Magnetohydrodynamics, 2009(2): p. 275–280

19. P. Zabiński, K. Mech, R. Kowalik, Co-Mo and Co-Mo-C alloys deposited in a magnetic field of high intensity and their electrocatalytic properties. Arch. Metall. Mater. **57**(1), 127–133 (2012)

20. P. Zabiński, K. Mech, R. Kowalik, Electrocatalytically active Co-W and Co-W-C alloys electrodeposited in a magnetic field. Electrochim. Acta **104**, 542–548 (2013)

21. P.R. Zabinski et al., Electrodeposited Co-Mo-C cathodes for hydrogen evolution in a hot concentrated NaOH solution. J. Electrochem. Soc. **150**(10), C717–C722 (2003)

22. S. Meguro et al., Electrodeposited Ni-Fe-C cathodes for hydrogen evolution. J. Electrochem. Soc. **147**(8), 3003–3009 (2000)

23. P.R. Zabinski et al., Electrodeposited Co-Fe and Co-Fe-C alloys for hydrogen evolution in a hot 8 kmol m-3 NaOH solution. Mater. Trans. **44**(11), 2350–2355 (2003)

24. P.R. Zabinski et al., Electrodeposited Co-Ni-Fe-C alloys for hydrogen evolution in a hot 8 kmol·m-3 NaOH. Mater. Trans. **47**(11), 2860–2866 (2006)

25. H. Vandenborre, P. Vermeiren, R. Leysen, Hydrogen evolution at nickel sulphide cathodes in alkaline medium. Electrochim. Acta **29**(3), 297–301 (1984)

26. F.H. Saadi et al., Operando synthesis of macroporous molybdenum diselenide films for electrocatalysis of the hydrogen-evolution reaction. ACS Catal. **4**(9), 2866–2873 (2014)

27. Kowalik, R., et al. Electrochemical deposition of Mo-Se thin films. in *ECS Transactions*. 2015

28. D. Merki, X. Hu, Recent developments of molybdenum and tungsten sulfides as hydrogen evolution catalysts. Energy Environ. Sci. **4**(10), 3878–3888 (2011)